Density Functional Study on Geometry and Electronic Structure of Nitrile Hydratase Active Site Model

W. NOWAK,[1,2] Y. OHTSUKA,[1] J. HASEGAWA,[1] H. NAKATSUJI[1]

[1]*Department of Synthetic Chemistry and Biological Chemistry, Faculty of Engineering, Kyoto University, Kyoto, Japan*

[2]*Institute of Physics, N. Copernicus University, ul. Grudziadzka 5, 87-100 Torun, Poland*

Received 17 September 2001; accepted 7 March 2002

DOI 10.1002/qua.10332

ABSTRACT: Nitrile Hydratase (*R. Sp. 771,* NHase, EC. 4.2.1.84, CAS registration no. 82391-37-5), the enzyme that plays an important role in the industrial production of acrylamide, is studied theoretically in this article. For the first time the electronic structure of the active site of nitrosylated form with a proper oxidation state of the cysteine ligands is calculated using the density functional theory (DFT) method with the Becke, Lee, Yang, and Paar (B3LYP)6-31G* functional. The optimized geometries of six and five coordinated complexes are different, showing that the photodissociation of NO triggers a substantial relaxation of the NHase active site. The major structural change is a shift of the position of iron with respect to the four equatorial ligands, which resembles a heme doming observed in myoglobins. Calculated charge distribution supports the role of Fe as a possible Lewis acid in catalytic cycle. We found that the cysteine-sulfinic residue (Cys112) is very strongly polarized in NHase. Sulfur atom S_γ Cys112 is predicted to be the most positively charged center. This result gives independent support to a very recent finding of the critical role of an oxidation in the position Cys112 for preserving catalytic activity of the enzyme (Endo, I.; Nojiri, M.; Tsujimura, M.; Nakasako, M.; Nagashima, S.; Yohda, M.; Odaka, M. J Inorgan Biochem 2001, 83, 247). Int J Quantum Chem 90: 1174–1187, 2002

Key words: B3LYP; DFT; enzyme catalysis; ferric complexes; oxygen claw setting

Correspondence to: W. Nowak, at the Institute of Physics; e-mail: wiesiek@phys.uni.torun.pl

Contract grant sponsor: Japan Society for the Promotion of Science

Contract grant sponsor: Polish State Committee for Scientific Research

Contract grant number: 6 P04A 06614

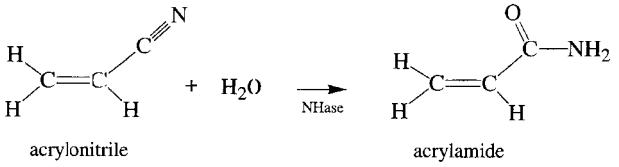

FIGURE 1. An example of the reaction catalyzed by nitrile hydratase.

Introduction

In recent years biotechnology has become one of the strategic areas of the research. Many useful products may be obtained in a cheap and efficient way using carefully selected bacteria. Biotechnological methods called "enzymation" are based on the chemical reaction catalyzed by the particular enzyme produced within a cell. The interest in catalytic activities of such enzymes stimulates interdisciplinary efforts aimed at elucidation of molecular mechanisms and their reactivity. The unique spatial arrangement and electronic properties of the active site of the protein are the most important factors determining possible applications of the molecule in biotechnology.

One of the best examples of the proteins that are "successful" in large scale chemical synthesis is nitrile hydratase (NHase, EC. 4.2.1.84, CAS registration no. 82391-37-5) [1]. The reaction catalyzed by NHases is hydration of nitriles to their corresponding amides. The example is shown in Figure 1.

Nitrile hydratase was discovered by Asano et al. in 1980, during their work on microbial degradation of acetonitrile [2]. In 1985 the industrial production of acrylamide using ferric NHase of *Rhodococcus sp.* N-774 was initiated in Japan (Nitto Chemical Industry; current name, Mitsubishi Rayon Co.) [3]. This enzyme was replaced by the second-generation nitrile hydratase catalyst obtained from *Pseudomonas chlororaphis* B23. Now NHase from *Rhodococcus rhodochrous* J1 (with low spin Co^{3+} in active site) is being used in large-scale production (30,000 tons per year) of acrylamide [4, 5]. These enzymes, due to their selectivity toward aromatic and aliphatic substrates, may be also used for the synthesis of other useful chemicals. The enzyme from *R. rhodochrous* J1, with different preparation of bacteria, serves as a catalytic medium in the industrial production of nicotinamide from 3-cyanopyridine [5]. New applications of NHase from *Pseudomonas putida* in stereoselective synthesis are anticipated [6]. Moreover, compounds useful in the pharmaceutical industry may be obtained with the help of these metalloenzymes [7]. The NHases are also good potential candidates for environmental biodegradation of acrylonitrile and nitrile herbicide contaminations [8, 9].

An interesting phenomenon related to enzymatic activity is photosensitivity of NHases. Some iron-containing NHases—for example, isolated from *Rhodococcus sp.* N-771 (*R. sp.* N-771) [10] and from *Rhodococcus sp.* R312 [11]—lose their activity after incubation of microorganisms in the dark but recover catalytic abilities upon light irradiation. Noguchi et al. presented evidence that this light-controlled switching between an active and the inactive state is related to the presence of the endogenous nitric oxide (NO). Upon irradiation, NO photodissociates and the enzyme becomes active [12, 13]. The electronic mechanism of the NO photolability is not known [14]. The list of photoreactive proteins is rather short, so this phenomenon stimulates an additional interest in the electronic structure studies of the NO–NHase complexes. In the future, such photo-controllable proteins may be core systems of nanodevices.

The NHases are composed of two subunits, α and β, with MW around 23 kD each. They contain one iron atom per $\alpha\beta$ unit. Iron is 5-coordinated, exclusively by aminoacids from the α subunit. The sixth coordination position may be occupied, for example, by H_2O or NO. The active site is located in a cavity at the subunit's interface. The first solved crystal structure of NHase (from *Rhodococcus sp.* R312, resolution 2.65 Å) revealed a novel iron center with a structure not previously observed in proteins, having an S_3N_2X ligand sphere [15]. Important insights were provided by the recent X-ray study of the structure of NHase–NO complex (*R. sp.* N-771) published by Nagashima et al. [16]. The higher-resolution data (1.7 Å), combined with results of Fourier transform ion cyclotron resonance mass spectrometry, indicate that two of three coordinating cysteine residues are posttranslationally oxidized to cysteine–sufinic acid (Cys112 SO_2H) and cysteine–sulfenic acid (Cys114-SOH) [16]. A recent study shows that posttranslational modification is essential for catalytic activity of NHase [17].

The Electron Paramagnetic Resonance (EPR) spectra indicated that iron in the nitrosilated NHase (inactive form) is in the low spin ferric state [18]. The recent EXFAFS (extended X-ray absorption fine structure) studies of the inactive NHase and of some model compounds are consistent with this notion [19]. The low spin nonheme ferric com-

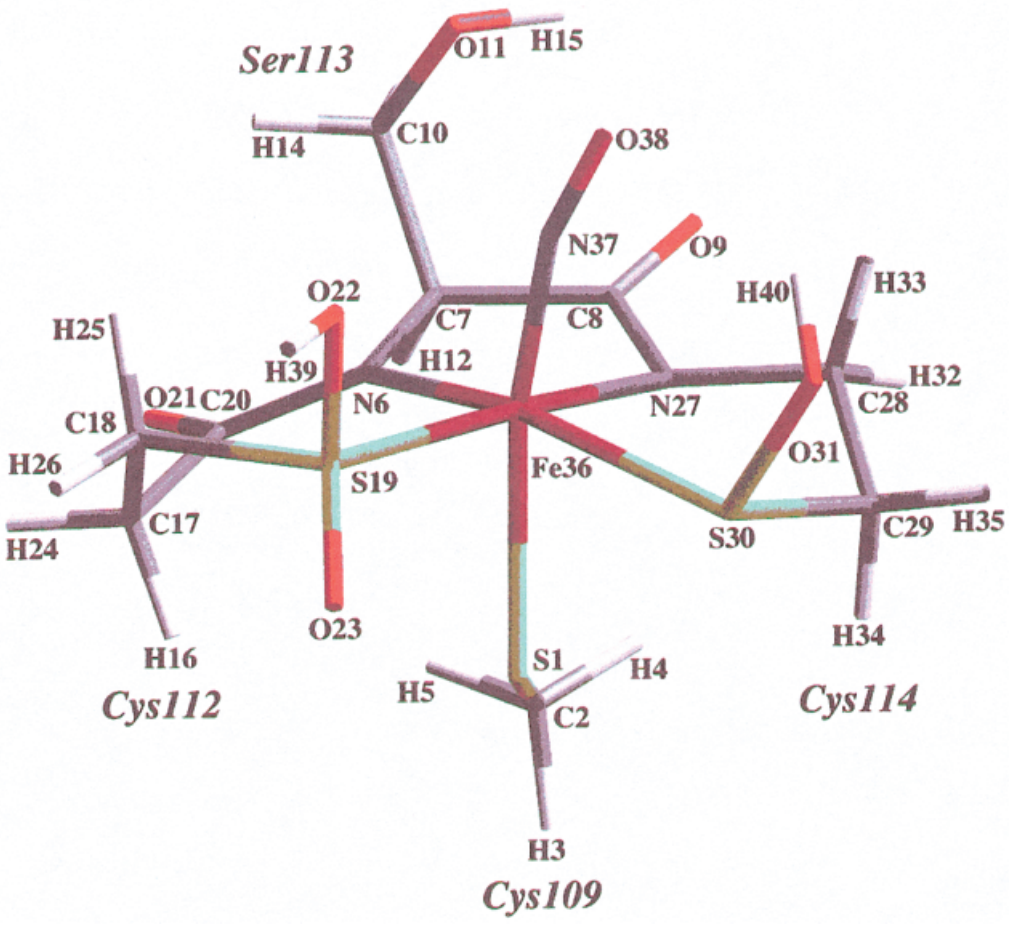

FIGURE 2. The structure of 6c NOsNHase model of nitrile hydratse active site (DFT/B3LYP optimized geometry).

pounds with the NO ligand are rare [20] and were not studied theoretically.

The goal of the current research was to find out what structural changes are related to the NO inactivation of NHase. We determined an electronic structure of low spin Fe(III) states of 6- and 5-coordinated (6c, 5c) models of the N-771 NHase active site. Changes in the electronic structure induced by the NO ligation/dissociation were examined. In particular, the nature of the NO ligand binding to the iron center model is described. This Fe—NO bond is broken by absorption of light, being thus a localized trigger of the enzymatic activity.

The high-resolution X-ray study [16] revealed in the *R. sp.* N-771 NHase active site an unusual triangular arrangement of three oxygen atoms [the so-called "claw setting": O_γ (Ser113), O_δ (Cys114), $O_{\delta 1}$ (Cys112); see Fig. 2]. These oxygens were postulated to play an important role in the stabilization of NO bound to NHase [16]. It is worthwhile to note that the NO–NHase complex is stable (in dark and anaerobic conditions) for over a year, which is rather unusual for Fe(III)–NO compounds. We therefore paid particular attention to possible interactions of these three specifically arranged oxygen atoms with the NO molecule.

To our knowledge, no electronic structure calculations of the NHase active site were published so far. The cysteine–sulphenic (Cys-SOH) and cysteine-sulphinic groups (Cys-SO_2H) coordinating to the iron center are also theoretically studied in this work for the first time. We hope that data presented here will be helpful in explanation of a mechanism of the catalytic activity of NHases.

Methods

MODEL STRUCTURE

A model of the enzymatic active site used in the calculations (NO-coordinated NOsNHase) is pre-

sented in Figure 2. The central atom is Fe(III) iron. It is coordinated by the sulfur S_γ atom of Cys109 (S1), the amide nitrogen of Ser113 (N6), the sulfur S_γ atom of cysteine–sulfinic acid (S19, Cys112-SOH2). Two other coordinating atoms are amide nitrogen and sulfur, both from cysteine–sulfenic acid (N27, S30, Cys114-SOH). To perform ab inito calculations, the number of atoms has to be reasonably small. Therefore, in our model, two peptide bonds from the α subunit polypetide chain have been cut (X′-Cys112, Cys114-X″) and C and N "terminal" atoms participating in these bonds have been replaced by the hydrogen atoms H16 and H32, respectively. The Cys109 residue is reduced to the SCH_3 mercaptide group (see Fig. 2). We call this model sNHase. The initial structure for the geometry optimization was the same as the recent X-ray structure of the inactive form of NHase (*R. sp.* N-771; pdb code, 2AHJ; resolution, 1.70 Å) by Nagashima et al. [16]. In this structure the NO molecule is the sixth ligand, so it was included in the 6-coordinated model, as well (NOsNHase). Hydrogen atoms were added using Cerius2 software [21]. Initial orientations of the important $O\delta_1$—H, $O\delta$—H, and $O\gamma$—H bonds were set in accordance with a possible hydrogen bond network reported for enzymes studied [22].

Calculations were performed for low spin ferric complexes, for example, for singlet states of 6-coordinated species and for doublet states of 5-coordinated species. These spin states of *R. sp.* N-771 enzyme were postulated on the basis of the EPR spectra [23].

COMPUTATIONAL METHOD

In this density functional theory (DFT) study a standard 6-31G* basis set as implemented in Gaussian 99 (Rev. A8) software package [24] was used to represent Kohn–Sham molecular orbitals (KSMO). The total number of gaussian basis functions (NOsNHase 6c model) was 388. The hybrid-type exchange-correlation potential Becke, Lee, Yang, and Paar (B3LYP) [25, 26], which was used in the calculations, is defined as

$$V_{xc} = (1 - A)*E_X^{Slater} + A*E_X^{HF} + B*E_X^{Becke} + C*E_C^{LYP} + (1 - C)*E_C^{VWN} \quad (1)$$

where E_X^{Slater} is the Slater exchange potential, E_X^{HF} is the Hartree–Fock (HF) exchange, E_X^{Becke} is a gradient correction to the exchange introduced by Becke [27], E_C^{LYP} is the Lee–Yang–Parr correlation potential [28], and E_C^{VWN} is Vosko–Wilk–Nusair correlation potential [29]. Constants A, B, and C were obtained by fitting the theoretical results to the experimental heats of formation [25]. The B3LYP potential has been previously used successfully in DFT studies of large bioinorganic molecules (see, e.g., Ref. [30]).

Results and Discussion

The main focus in this work was to study possible structural rearrangements of the NHase active site induced by the NO binding/photodissociation. This reaction is critical for restoring activity of the enzyme. The optimized geometries of the iron center of the active (5c) and the inactive (NO, 6c) forms are presented in Table I.

It is interesting to estimate binding energy of NO to the NHase active site model. Because calculations of full NO binding curves for a system of this size are computationally very demanding, a simple estimation was done by a comparison of total energy of the low spin states of the 6c model (NOsNHase) with the sum of energies of the 5c complex (sNHase) and the NO ligand. To avoid problems with a spin contamination the restricted open-shell Kohn–Sham B3LYP scheme (RKS) was used to calculate energies. Results are presented in Table II.

The total energies of the active site model with the experimental geometry adopted from the structure of the whole protein were also calculated (see Table III). These data give useful estimation of the energy of the NHase structural "doming" that is observed after the dissociation of the NO ligand. For comparison, in both tables the data obtained with the HF method and Huzinaga's 2DZP type basis set (364 Gaussian functions; results are to be published elsewhere) were also included.

For iron ion, Huzinaga's set (5333/53/5)/[533111/521/311] was used [31] together with two p-type 0.038, 0.118 functions, one d-type flexible function (ξ = 0.1133) by Hay [32] and one set of f-type double ξ Roos' augumented-ANO [33]. Nitrogen and oxygen of NO were described by (63/5)[5121/41] plus anion p-type functions proposed by Dunning and Hay [34] (ξ = 0.048) and two d-type polarization functions (N: ξ_1 = 0.412, ξ_2 = 1.986; O: ξ_1 = 0.535, ξ_2 = 2.704) [31]. For C, N, and O atoms, (63/5)[321/41] sets were used. On the nitrogen's atoms coordinated to the iron center, one

TABLE I

Optimized geometries of 5c and 6c models of NHase active center.[a]

	5c DFT	6c DFT	6c Exp [16]
Bond lengths in the coordination sphere of iron (in Å)			
Fe-N37 (NO)		1.639	1.65
Fe-S1 (S_γ Cys109)	2.198	2.346	2.30
Fe-S19 (S_γ Cys112)	2.226	2.300	2.26
Fe-S30 (S_γ Cys114)	2.367	2.352	2.33
Fe-N27 (Cys114)	1.841	1.926	2.05
Fe-N6 (Ser113)	1.876	1.935	2.09
N37-O38 (NO)		1.161	1.33
S1-C2 (S_γ-C_β Cys109)	1.835	1.828	1.80
S19-O22 (S_γ-$O_{\delta1}$ Cys112)	1.691	1.667	1.51
S19-O23 (S_γ-$O_{\delta2}$ Cys112)	1.481	1.479	1.41
S30-O31 (S_γ-O_δ Cys114)	1.693	1.697	1.51
C7-C10 (C_α-C_β Ser113)	1.546	1.542	1.54
C10-O11 (C_β-O_γ Ser113)	1.421	1.428	1.43
C7-C8 (C_α-C Ser113)	1.519	1.525	1.53
C8-O9 (Ser 113)	1.231	1.237	1.23
C8-N27 (C Ser113-N Cys114)	1.371	1.353	1.33
N27-C28 (N-C_α Cys114)	1.464	1.455	1.47
C28-C29 (C_α-C_β Cys114)	1.521	1.523	1.52
C29-S30 (C_β-S_γ Cys114)	1.826	1.845	1.82
N6-C20 (N Ser113-C Cys112)	1.379	1.365	1.32
C20-O21 (Cys112)	1.230	1.236	1.23
C17-C20 (C_α-C Cys112)	1.534	1.533	1.51
C17-C18 (C_α-C_β Cys112)	1.533	1.530	1.52
C18-S19 (C_α-S_γ Cys112)	1.817	1.812	1.83
Selected atom–atom distances (in Å)			
O22-N37 ($O_{\delta1}$ Cys112-N(NO))		2.824	2.92
O22-O38 ($O_{\delta1}$ Cys112-O(NO))		3.120	3.05
O31-N37 (O_δ Cys114-N(NO))		3.062	2.81
O31-O38 (O_δ Cys114-O(NO))		2.973	2.76
O11-N37 (O_γ (Ser113-N(NO))		3.137	2.95
O11-O38 (O_γ Ser113-O(NO))		3.415	3.31
S30-N27 (S_γ-N Cys114)	2.883	2.921	2.97
S19-N6 (S_γ Cys112-N Ser113)	2.979	3.095	3.26
N6-N27 (N Ser113-N Cys114)	2.529	2.580	2.85
S19-S30 (S_γ Cys112-S_γ Cys114)	3.229	3.455	3.28
(Oxygen claw setting)			
O31-O22 (O_δCys114-$O_{\delta1}$Cys112)	2.993	4.153	3.38
O22-O11 ($O_{\delta1}$Cys112-O_γ Ser113)	4.515	5.210	5.432
O31-O11 (O_δCys114-O_γ Ser113)	5.278	5.950	5.564
Selected bond angles (deg)			
Fe36-N37-O38 (Fe-N-O)		161.4	158.6
Fe-S_γ-C_β (Cys109)	102.3	107.1	106.5
S19(S_γ Cys112)-Fe-N27(Cys114)	152.6	174.9	175.6
S30(S_γ Cys114)-Fe-N6(Ser113)	164.9	162.0	171.1
Fe-S_γ-$O_{\delta1}$ (Cys112)	100.7	107.7	115.6
$O_{\delta1}$-S_γ-$O_{\delta2}$ (Cys112)	107.6	108.3	107.1
Fe-S_γ-O_δ (Cys114)	105.6	112.8	107.8
Selected torsion angles (deg)			
χ_1 (Cys112)	50.8	50.7	49.6
χ_1 (Ser113)	70.5	76.6	68.1
χ_1 (Cys114)	−39.9	−48.12	−55.8
C_α-C_β-S_γ-$O_{\delta1}$ (Cys112)	146.6	157.1	176.6
C_α-C_β-S_γ-O_δ (Cys114)	−68.0	−84.7	−69.1

[a] Complete optimized geometries of 5c and 6c models may be obtained upon request from the corresponding authors.

TABLE II

Total energies of the lowest singlet and doublet states—DFT/B3LYP/6-31G* optimized geometries.

Method/basis	Total energy (au)			NO binding energy	
	NOsNHase (6c)	sNHase (5c)	NO[a]	ΔE (au)	ΔE (kcal/mol)
HF/basis-H[b]	−3491.825856	−3362.706274	−129.262659	−0.143077	−89.8 unstable
HF/basis-H[c]	−3491.825856	−3362.728918	−129.262659	−0.165721	−104.0 unstable
B3LYP/6-31G*[b]	−3502.049765	−3372.117287	−129.8829	+.049578	+33 bound
B3LYP/6-31G*[c]	−3502.049765	−3372.152327	−129.8829	+.0145	+9.1 bound

[a] The geometry of NO is the same as in the 6c optimized model compound (r(N—O) = 1.16 Å).
[b] The geometry of sNHase (5c) was not optimized—was taken from the optimized NOsNHase (6c).
[c] The geometry of both 6c and sNHase (5c) was fully optimized.

additional d-type polarization function was added (ξ = 0.864). For sulfur atoms, sets of (533/53)[53111/521] and one d-type (ξ = 0.421) plus Dunning and Hay anion p-type function (ξ = 0.041) [34] were used.

The mechanism of the catalytic activity of NHase is not known. In the two proposed models [1] iron plays the role of Lewis acid. The unusually oriented three oxygen atoms, forming a triangle around the pathway to the central iron, may also contribute to the activity of the enzyme. Therefore, it is important to study a charge distribution in both 5c and 6c forms. Mulliken charges calculated by the DFT/B3LYP method are presented in Table IV.

The calculated geometry of the 6c complex is in agreement with the X-ray structure of the inactive form of *R. sp.* N771 NHase [16] (see Table I). The central Fe—NO bond length of 1.639 Å obtained by the DFT method compares very well with the X-ray value of 1.65 Å. It is also close to the value of 1.68(3) Å estimated by Scarrow et al. [19] from the analysis of the iron K-edge X-ray absorption spectrum of the inactive form of NHase from *Rhodoccocus sp. R312.* The optimized Fe—N—O bond angle (161.4°) is very close to the experimental value (158.6°, Ref. [16]).

Calculated Fe—S bond distances are from 0.02 Å (S30, Cys114) to 0.05 Å (S1, Cys109) longer than those experimentally observed. Larger differences are observed in amide nitrogen-iron bond lengths: calculated values are 0.12 Å (N27) and 0.15 Å (N6) shorter than those found in the protein crystal. This finding suggests a stronger bonding of nitrogen atoms to Fe(III) in model compounds than that present in the protein. It is worthwhile to note that our calculated values of the Fe—N bond distances (1.926 Å and 1.935 Å) are close to the value of 1.954(2) Å measured in a low MW complex structure, which was synthesized recently by Noveron et al. [35] as a model of NHase. Moreover, the DFT values are not far from the range of 1.944(4)–2.031(12) Å Fe(III)-N_{por} distances found in a series of 23 ferric porphyrins [36].

The differences in the calculated Fe—N (short) and Fe—S (Cys112, Cys114, long) bond lengths are expected, because the deprotonated amides are strong σ donors, while sulfenic and sulfinic residues are π donors.

Special attention should be devoted to the calculated S—O distances in cysteine-sulfinic (Cys112) and cysteine-sulfenic groups (Cys114), which are much larger than the experimental ones. The difference is 0.07 Å for S19-O23 (S_γ-$O_{\delta 2}$ Cys112) and 0.16 and 0.19 Å for S19-O22 (S_γ-$O_{\delta 1}$ Cys112) and S30-O31 (S_γ-O_δ Cys114), respectively. All these oxygen atoms appear in the active site region as a result of the posttranslational oxidation of Cys112 and

TABLE III

Total energies in (au) of the lowest calculated singlet and doublet states—X-ray (pdb) rigid geometry of the active site.

Method/basis	NOsNHase	sNHase	NO[a]	ΔE (a.u.)[b]	ΔE (kcal/mol)[b]
HF/basis-H	−3491.381451	−3362.360653	−129.199006	−0.178208	−111.8 unstable
B3LYP/6-31G*	−3501.614760	−3371.721360	−129.840381	+0.05302	+33.3 bound

[a] A geometry of NO used is the same as in protein structure (r(N—O) = 1.33 Å pdb).
[b] $\Delta E = ([E_{5c} + E_{NO}])-E_{6c})$ denotes an estimation of the bond dissociation energy.

TABLE IV

The DFT Mulliken charges on atoms of 6-coordinated inactive form (NONHase) and 5-coordinated active form (NHase) of the NHase models.

Atom	6c	5c	ΔQ = 6c–5c[a]
1 S	−0.152	−0.125	−0.027
2 C	−0.589	−0.609	0.019
3 H	0.184	0.187	−0.003
4 H	0.200	0.206	−0.006
5 H	0.208	0.212	−0.004
6 N	−0.584	−0.618	0.033
7 C	−0.043	−0.040	−0.003
8 C	0.507	0.525	−0.018
9 O	−0.512	−0.486	−0.026
10 C	−0.029	−0.038	0.008
11 O	−0.635	−0.626	−0.009
12 H	0.183	0.182	0.001
13 H	0.146	0.147	−0.001
14 H	0.165	0.170	−0.006
15 H	0.414	0.413	0.002
16 H	0.220	0.224	−0.004
17 C	−0.405	−0.417	0.013
18 C	−0.486	−0.489	0.003
19 S	0.973	0.921	0.052
20 C	0.536	0.552	−0.016
21 O	−0.489	−0.463	−0.026
22 O	−0.670	−0.694	0.024
23 O	−0.522	−0.524	0.003
24 H	0.195	0.198	−0.003
25 H	0.233	0.237	−0.004
26 H	0.209	0.212	−0.004
27 N	−0.564	−0.606	0.042
28 C	−0.133	−0.110	−0.024
29 C	−0.460	−0.485	0.025
30 S	0.495	0.446	0.049
31 O	−0.703	−0.706	0.003
32 H	0.197	0.180	0.017
33 H	0.151	0.187	−0.036
34 H	0.228	0.230	−0.002
35 H	0.205	0.207	−0.003
36Fe	0.492	0.483	0.009
37 N	0.154		
38 O	−0.203		
39 H	0.444	0.442	0.002
40 H	0.440	0.473	−0.032

[a] Defined as 6c–5c difference and represent a charge reorganization upon NO dissociation from the active site.

Cys114 residues. Oxygen atoms O23 and O31 constitute a part (together with O11 from Ser113) of the so-called "oxygen claw setting." This triangular arrangement of oxygen atoms was postulated by Nagashima et al. [16] to play a role in stabilization of the NO binding. On one hand, the observed discrepancy between the calculated and observed bond lengths may be attributed to difficulties in a proper description of sulfur atoms by a relatively small 6-31G* basis adapted in current calculations. On the other hand, this difference may indicate that the protonation states of residues Cys112 and Cys114 in the inactive form of NHase are different from those suggested in the article [16]. Cysteine-sulfenate and cysteine-sulfinate groups are strong acids. For example, pKa = 1.50 for cystein–sulfonic acid [37]. It is therefore probable that one or two residues are in their anionic forms while in a protein environment. Therefore the S—O^- distances are expected to be shorter than the S—OH distances calculated here. In a recently published structure of an anionic NHase model compound [38], the average S—O bond distance is 1.472(4) Å, which compares very well with the average value of 1.477 Å observed in the NHase protein structure [16]. It is thus possible that negatively charged SO^- groups are instrumental in a mechanism of catalytic activity of this enzyme.

The covalent bond lengths between heavy atoms of the polypeptide chain of the 6c sNHase model are in very good agreement with experimental data. The average difference for 14 bonds is 0.013 Å. The largest deviation is observed in N6—C20 peptide bond, which is 0.05 Å too long.

Bond angles of the organic ligand correspond nicely to the structure of the active site extracted from the protein. In general, differences do not exceed a few degrees. Rather large differences of 8–9° [S_γ (Cys114)-Fe-N(Ser113), Fe-S_γ-$O_{\delta 1}$ (Cys112)] are perhaps connected with the more open structure of the oxygen claw setting present in the DFT 6c geometry than those in protein crystal. Also the calculated torsional angles are in a satisfactory agreement with the experimental ones, especially for the side chain orientations determined by the χ_1 angles. The largest differences of 20° and 16° are in C_α-C_β-S_γ-O_δ torsional angles of oxidized cysteine residues and are related to a notable increase of distances between the three claw oxygens. For example, the optimized O31–O22 distance is 0.77 Å larger than that observed in the protein. Such relaxation was expected, because in our model we did not include water or any further protein atoms. In particular, no atoms from Arg56 residue of the β subunit, which perhaps affect the geometry of the active site by a network of hydrogen bonds [22], were present.

Thus, our data indicate two things: (1) the active site of NHase possesses a certain level of flexibility, which probably facilitates the binding of a substrate or water; and (2) the effect of hydrogen bonds on the geometry of the oxygen claw setting in 6c complex is not particularly large. However, it would be interesting to compute the influence of the small changes in Cys112 (and Cys114) geometry on the electronic structure of the NHase active site. We have already initiated such study. One may expect that intersubunit α–β interactions affect in this way catalytic properties of NHases. The location of the active site exactly on the border between two subunits offers a possibility for such control. It may be that the observed architecture of these enzymes is not accidental.

The closest contact between the oxygen atom of NO and the oxygen claw setting atoms measured in the crystal is 2.75 Å (O31, Oδ from Cys114). In the optimized 6c structure, the same O31 oxygen remains also to be the closest neighbor to the ligand, but the distance is 2.97 Å. The proton from the SOH group (Cys114) points toward the oxygen atom of NO, making an intramolecular hydrogen bond O_δ-H . . . O(NO), which contributes to the observed unusual stability of the NO–NHase complex [16].

Our DFT data give an opportunity to study structural rearrangements of the NHase active site model after the photodissociation of NO (Table I). The most pronounced effect in the calculated bond lengths is shortening of the Fe—S1 (Sγ Cys109) bond distance from 2.346 Å to 2.198 Å in the 5c complex (Δr = 0.148 Å). This is a clear manifestation of the strong NO transeffect present in the system. The same distance measured in the crystal in dark (NO attached) and light conditions (NO "dissociated" but located close to Fe, r(Fe-NO) = 1.66 Å) decreases from 2.30 Å to 2.25 Å [22]. Experimental study [20] shows that positional differences in coordination sphere of the active center does not change more than 0.2 Å between light and dark conditions. Except for the Fe—S1 distance, which was discussed above, the changes in the bond lengths in our model do not exceed 0.1 Å. In our opinion, some further relaxation of the 5c NHase in solution may be required to restore its enzymatic activity.

Despite similar bond distances, the 6c (inactive) and 5c (active) structures are different. The main reason is a large shift in the position of the iron upon the dissociation of the NO ligand. This structural change may be qualitatively compared to the heme doming effect, typically observed in hemoglobins and in myoglobins [39] when the Fe—O_2 ligand bond the active site of the heme protein is broken. In fact, in the 6c optimized structure, the position of the iron atom is slightly above the (N6, N27, S19, S30) plane ("negative doming"). In the 5c model, the iron is clearly located below this plane. This effect is schematically presented in Figure 3, where the two nearly perpendicular cross-sections of the sNHase optimized structures are shown. The shift in the position of iron is 0.6 Å. This value is close to the values of iron displacements observed in heme proteins (0.4–0.6 Å [39]). However, such correlation is accidental, because one should note that in heme ferrous complexes, two factors play a role. The first part of doming is induced by the change of spin of iron from the low-spin state (singlet or doublet in 6c hemes) to the high-spin one (quintet in deoxy forms) and the other part by a strain from the proximal side protein helix. In our model of NHase we do not include any protein pull, and the spin state changes only from singlet to doublet.

Unfortunately, the structure of the so called "active" form of *Rhodococcus sp.* R312 NHase by Huang et al. [15] cannot be used to argue for the support of this theoretically predicted important structural change. The reason is its low resolution (2.65 Å). It is even possible that the data of Huang et al. were collected from the 6c structure, where the sixth ligand is water or OH^- hydroxide ion. Therefore, further high-resolution structural studies of NHases are highly desirable.

The catalytic properties of NHase are related to a particular electric field in the active side. Theoretically calculated charge distributions, despite their known shortcomings, are helpful in a qualitative discussion of the mechanism of the catalysis. The Mulliken charge distributions in 5c and 6c forms are presented in Table IV. In 6c species both amide nitrogens coordinated to Fe have almost the same negative charges, of −0.56–−0.59 (in e units). The axial Cys109 sulfur, also a σ donor, is less negatively charged (−0.15). Two carbonyl groups, C8-O9 and C20-O21, are strongly polarized (+0.5, −0.5). Their oxygen atoms interact with the protein surrounding and may form the hydrogen bonds. All three oxygen claw setting atoms: O11 (O_γ Ser113), O22 ($O_{\delta 1}$ Cys112), and O31 (O_δ Cys114) exhibit large negative charges. The charge of the Ser113 side group oxygen O11 (−0.64) is slightly lower than that of the cysteine–sufinic and cysteine–sulfenic residues (−0.67 and −0.70, respectively). The DFT Mulliken charges of protons

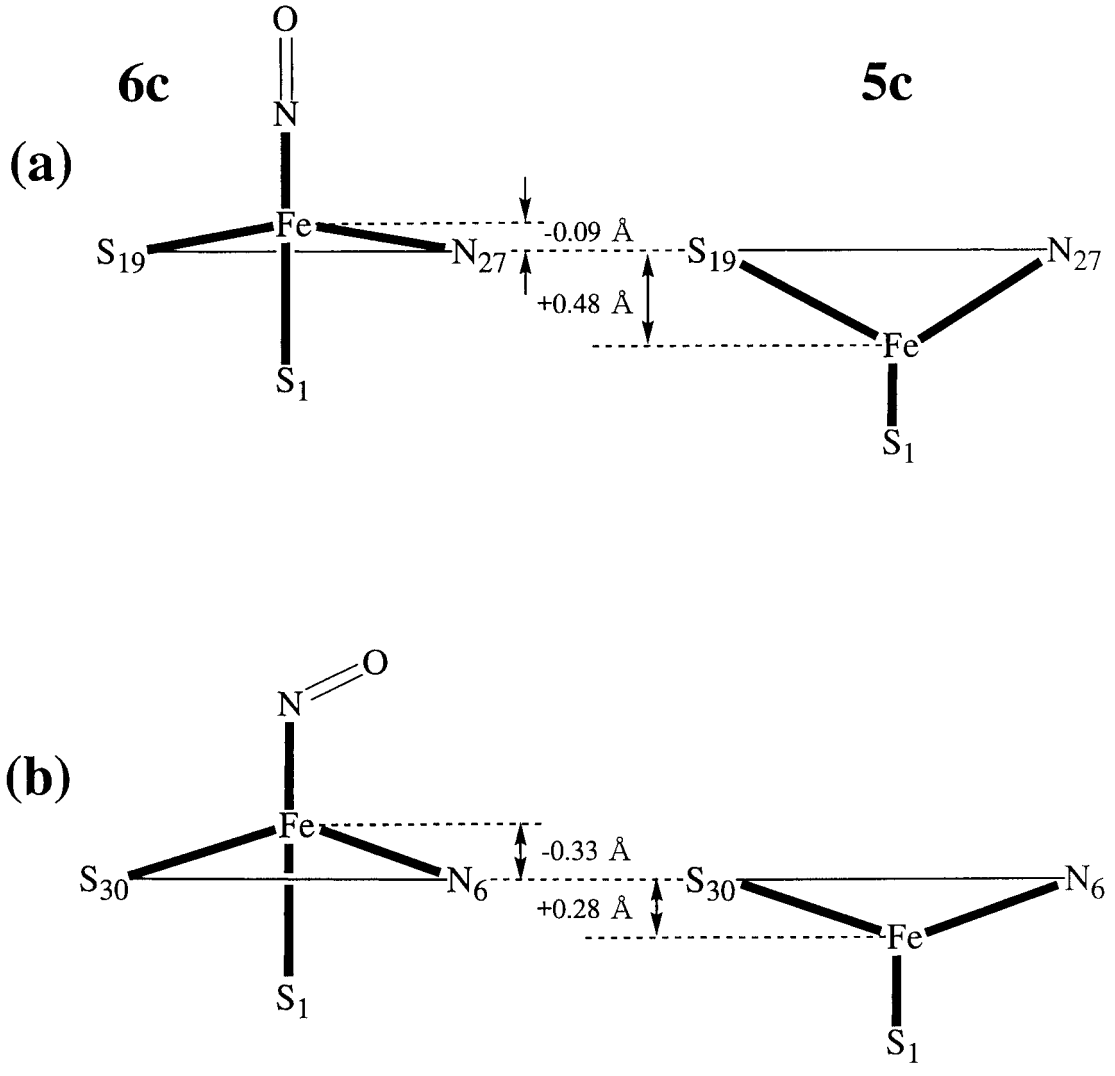

FIGURE 3. Schematic representation of major structural differences between optimized structures of NOsNHase (6c) and sNHase (5c) observed in the two nearly perpendicular planes: S19-Fe-N27 (a) and S30-Fe-N6(b). The NO ligand is located in plane (b).

bound to these oxygen atoms are similar, so no preference for a dissociation of a particular proton was found in our calculations.

The sulfur atom from cysteine-sulfenic residue (S30, Cys114) is moderately positively charged (+0.5), but charge depletion on the sulfur from the cysteine–sulfinic group (S19, Cys112) is as large as +0.97. Such strong polarization of this oxidized cysteine residue indicates its role in catalytic activity of the NHases. It is interesting to note that a recent study by Endo et al. [42] on recombinant NHases suggests that the modification of α-Cys112 into Cys-SO_2H is essential for the catalytic activity of Fe-type NHase. Mutations of Arg56 in β subunit decrease substantially the activity of the enzyme [43].

It has been proposed (see, e.g., Ref. [19]) that the iron ion may play the role of Lewis acid during the catalytic cycle. The DFT Mulliken charges close to +0.5 found on the central Fe ion (formally Fe^{+3}) only partially support this conjecture. One should note, however, that Mulliken charge distribution is basis-set–dependent and only changes in these numbers have more qualitative predictive value. We compared those charges calculated in 6c and 5c models. The changes are not large. In 6c complex, a negative charge on S1 (Cys109) is 0.03 larger than in 5c

complex, while the negative charge on N6 decreases by 0.03. On both S19 and S30, positive electronic charges decrease by 0.05 upon NO photodissociation. Interestingly, the Fe DFT charge is almost unaffected by the change of coordination.

The net charge on the NO ligand calculated by DFT/B3LYP method in the optimized complex is −0.05, indicating that the Fe—NO (neutral) model of bonding is adequate. Note however, that the N—O distance observed in the protein structure is 1.33 Å and not 1.16 Å, as found here. Our calculations (data not shown) performed for such X-ray geometry resulted in −0.25 charge on the NO ligand. Only a substantial π backdonation and a negative-ion type of ligation to the ferric iron atom may justify such an unusually large N—O bond length. Indeed, as we show below, even in this structure with the shorter NO bond, the backdonation is observed.

The selected KSMOs are presented in Figures 4 and 5 (contour level 0.05 was used for Molden [40] graphical display). For the purpose of further discussion, the molecular frame axes are defined approximately as follows: **x**: Fe-SCys112; **y**: Fe-SCys114; **z**: S109-Fe. Frontier electron spin density distribution in 5c sNHase doublet state is the following: Fe 0.80, S1 0.09, N6 0.03, N27 0.02. Thus, in the 5c system, a single electron is localized on the iron atom, which indicates that the iron atom is an active site. The singly occupied molecular orbital [SOMO; Fig. 4(b)] is an antibonding combination of Fe d_{yz} and S1 (Cys109) p_y atomic orbitals, indicating that π-type interaction is preferred in the course of the reaction with this iron ion.

The HOMO of this complex [Fig. 4(c)] is delocalized and has several main components: S1p_y, Fe d_{yz} + NO π^*_ψ, and a nonbonding type fragment localized on atoms N6-C20-O21, which form a peptide bond between Cys112 and Ser113 residues. Some contributions from p orbitals of the oxygen claw setting atoms O11(Ser113) and O31(Cys114) are also present. The lowest unoccupied molecular orbital (LUMO) of the 5c system presented in Figure 4(a) clearly has an S1—Fe antibonding σ character.

In the interpretation of the low-lying, low-intensity 710-nm band of the active form of NHase, a charge transfer **S** → Fe character is often proposed [41]. If our 5c system is an adequate model of this protein, then the axial Cys109 is probably involved in this electronic transition. However, the SOMO → LUMO excitation would lead to a charge transfer from Fe to S, so perhaps a low-energy band has a HOMO → LUMO nature. Symmetry Adapted Cluster-Configuration Interaction (SAC-CI) calculations on the electronic spectrum of model compounds should be helpful in clarifying this issue. Such calculations are under way.

Main features of HOMO of the 6c system are similar to those of 5c. The largest contribution comes from the nonbonding type MO of the Cys112–Ser 113 peptide bond atoms N6-C20-O21. We observe also [Fig. 4(f)] a bonding contribution to HOMO from Fe d_{yz} and NO π^*_ψ orbitals. The LUMO and LUMO1 [Fig. 4(e)] are clearly composed of NO π^*_ζ − Fe d_{xz} and NO π^*_ψ − Fe d_{yz} antibonding combinations. Also, LUMO2 shown in Figure 4(a) has a clear antibonding character with respect to all Fe-ligand bonds, including NO. This set of low-lying MOs, having strong antibonding character along the Fe-NO axis, may explain a particularly large photolability of NHase NO complexes [10]. Recent experiments show that not only *R. sp.* N771 is photoactivated, but also other enzymes from this family, for example NHase from *Comamonas testosteroni NI1,* easily lose NO upon light irradiation [11].

The nature of the S1—Fe bond is illustrated in Figure 5(a)–(c). An orbital #94 illustrates the σ–σ donation from S1 to Fe. The π_S–π_{Fe} donation is shown in Figure 5(b). An interaction that we would classify as "nonbonding" is presented in Figure 5(a) (HOMO1). One of the initial goals of this study was to search for electronic structure arguments for large stability of NO–ferric complexes. Thus, in Figure 5(d)–(f) the Fe—NO bonding is shown in detail. The main contribution to the NO bonding comes from a σ bond [MO #64, Fig. 5(f)]. This KSMO is of type 3σ(pz) NO + Fe d_{Z^2}. It is worth noting the stabilization, which comes from the H-bond to the O_δ fragment of Cys114. From the shape of the MO #65, one may expect that $O_{\delta 1}$ of Cys112 helps to keep the NO molecule in place by a delocalization of the NO $\pi^*\zeta$ molecular orbital. An interesting phenomenon is illustrated in Fig. 5(c). In MO #101 a backbonding from Fe $\pi_\psi(d_{yx})$ to π^*_ψ NO is clearly seen. Again, a large contribution from the Ser Oγ oxygen may help to stabilize NO in this complex. This effect leads to an enlargement of the N—O bond of NO.

In Table II, total energies of optimized models of active 5c form (sNHase) and inactive 6c form (NOsNHase) are presented. The HF method predicts that the sum of NO energy and sNHase is lower by 90 kcal/mol than that found for the NOsNHase complex. On the other hand, the DFT/

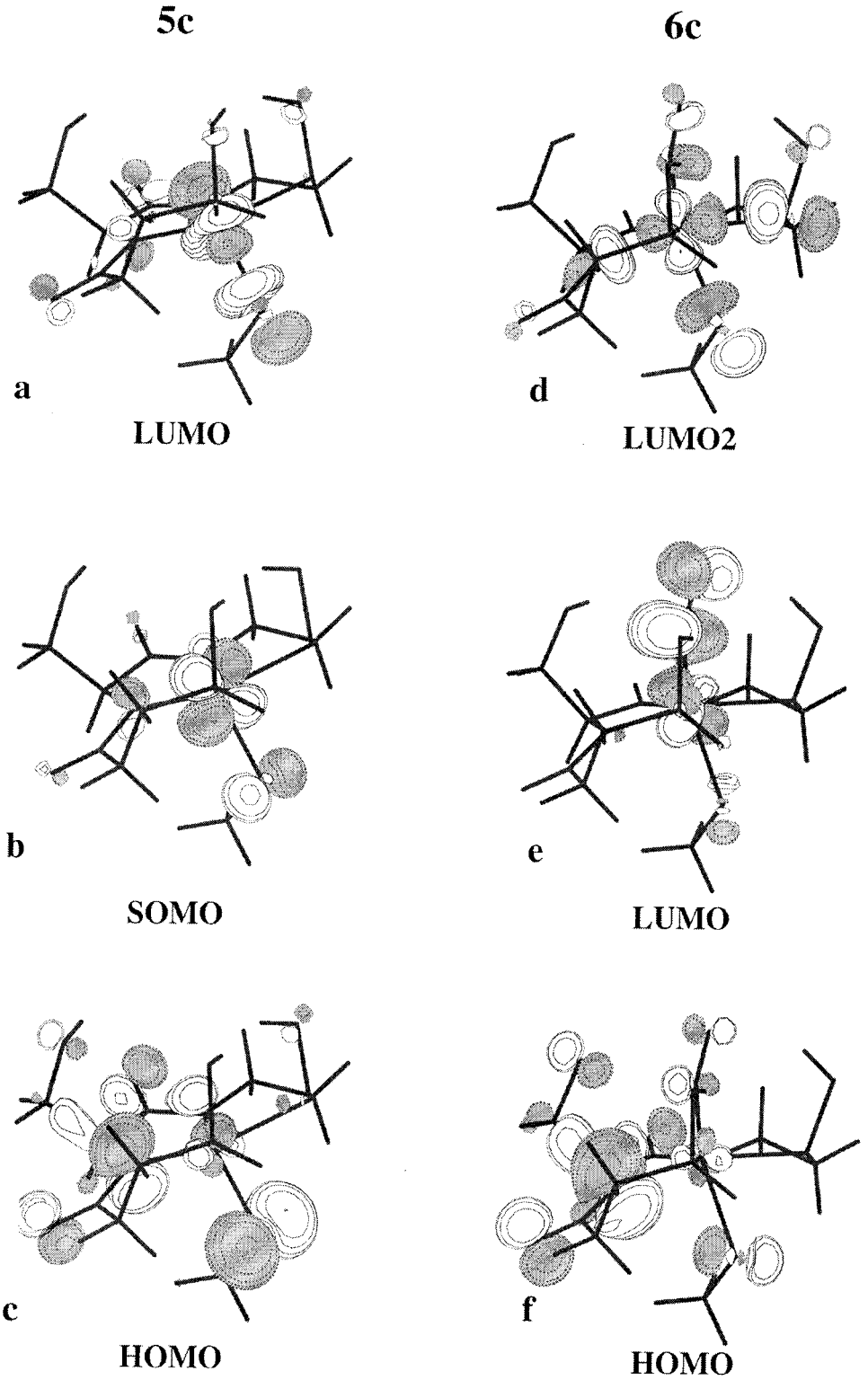

FIGURE 4. Contours of selected KS orbitals of NOsNHase (6c) and sNHase (5c).

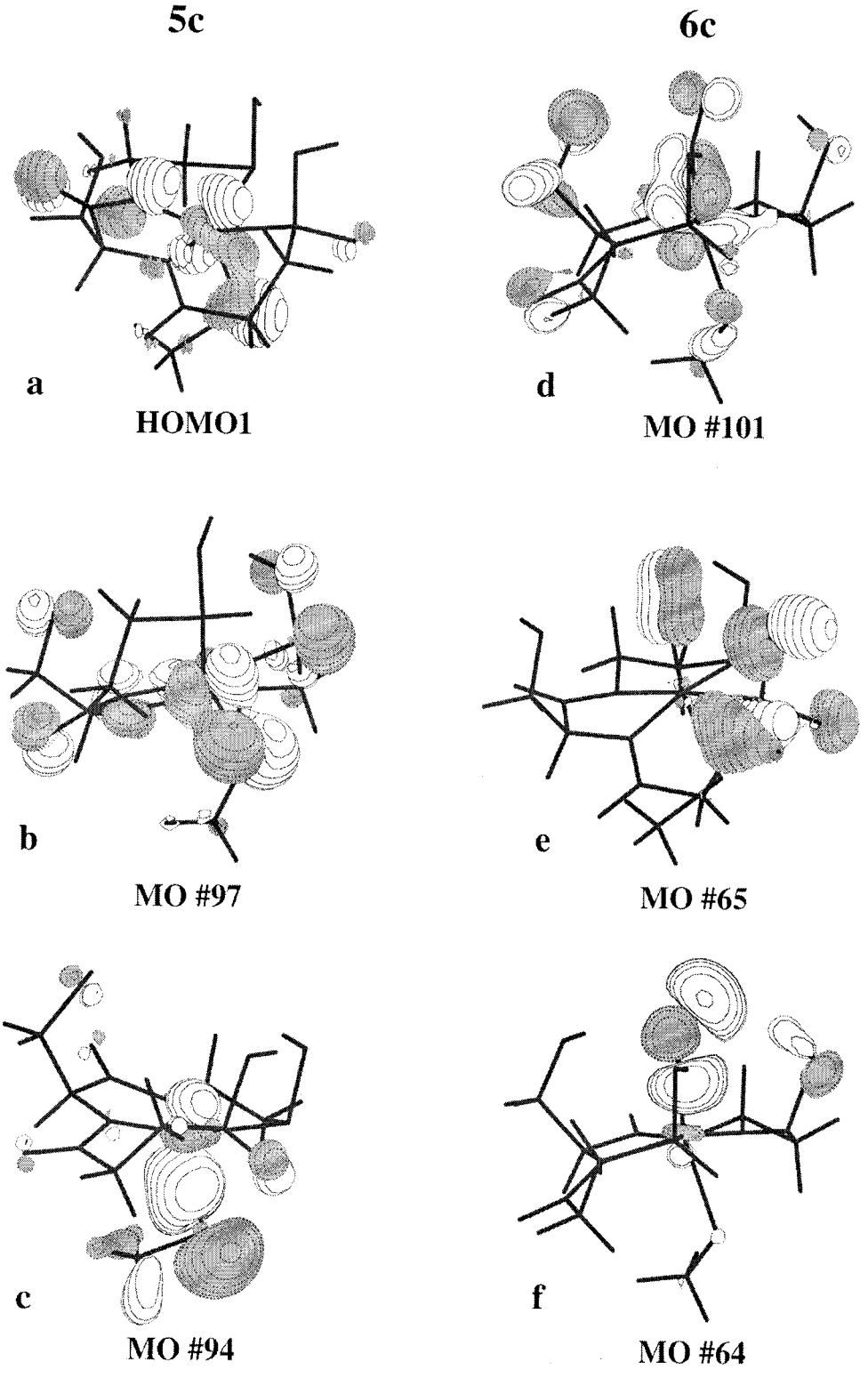

FIGURE 5. Contours of selected KS orbitals of sNHase (5c) showing the bonding between Fe and S1 (Cys109) (a, b, c) and the NO—Fe bonding in NOsNHase (6c) (d, e, f). HOMO1 denotes occupied MO next to HOMO. For details see the text.

B3LYP method gives a value of 9 kcal/mol as an estimate of the binding energy when the optimized geometry of the 5c complex is used. For the rigid X-ray structure (Table III) or for the rigid 6c optimized structure, the NO binding energy is estimated as 33 kcal/mol. No experimental data on NO binding energy in the enzyme are available yet. However, given the large stability of the NO complex in dark anaerobic conditions (over 1 year), one can conclude that the calculated value is an underestimate of the real binding energy. These data indicate, however, that the inclusion of correlation energy is essential in a qualitative description of the energetics of the NHase active site.

Using data from Table II, it is possible to estimate the amount of energy released during "NHase doming" observed in the 5c optimized structure. The relaxation from 6c DFT optimized geometry to the fully optimized 5c geometry gives 24 kcal/mol. One may expect that the protein active site is more rigid than molecular models used in the present study, but this large value indicates the possibility that the binding process of NO (or nitrile substrate) is not barrierless.

Conclusions

The geometry and electronic structure of low-spin ferric models of nitrile hydratase *R. sp.* N771 has been studied. For the first time, cysteine amino acids oxidized to cysteine–sufenic (Cys-SOH) and cysteine–sufinic acids (Cys-SO_2H) were included in the models. We found that DFT/B3LYP/6-31G* optimized geometry of the complex of sNHase with NO as the sixth ligand is close to the structure observed in protein crystal. The polypeptide chain structure is described very well by the DFT method. The largest differences were found in sulfur bonds. This element is difficult to describe theoretically, so in future studies, perhaps larger basis sets should be used on these atoms.

Our data indicate that the NO photodissociation triggers a substantial relaxation of the NHase active site. The major structural change is a shift of the position of iron with respect to the four equatorial ligands (see Fig. 3). This structural change resembles the heme doming observed in 5c myoglobins upon NO photodissociation. This structural transformation is an important finding, because if such rearrangement is experimentally confirmed it would open the way for regulation of the enzymatic activity of NHases by making mutations on the "proximal" side of the iron (residues 109, 108, and those with close contacts).

Calculated charge distribution corroborates the role of Fe as a possible Lewis acid in the catalytic cycle of the enzyme. We found, however, that the cysteine–sulfinic residue (Cys112) is very strongly polarized in this system. Sulfur atom S_γ Cys112 is predicted to be the most positively charged center. This result supports well a recent finding of the critical role of an oxidation in the position Cys112 for preserving catalytic activity of the enzyme [42].

Nitric oxide binding to the Fe^{+3} center is based on a classical [3σ(pz)NO-d_Z2 Fe] σ bond and a substantial Fe $d\pi$-NOπ^* backdonation. Low-lying (LUMO, LUMO1) NO-Fe antibonding orbitals may explain an easy photodissociation of this ligand from the NHase active site. It would be interesting to calculate the electronic structure of cobaltous NHases and to compare it with the present data, because such NO-inactivated enzymes do not exhibit photosensitivity. The DFT calculated binding energy of NO is at least 9 kcal/mol. The unusual stability of the NO-NHase complex is related more to a good steric shielding by the three oxygen claw setting atoms than to a particularly strong chemical bond to the ferric nonheme iron center.

The protonation state of the oxidized cysteine residues is still an open issue, so in the future, theoretical data for charged models will be presented. Such a study is in progress in our laboratory.

ACKNOWLEDGMENTS

W.N. expresses his gratitude to Japan Society for the Promotion of Science for generous funding of this research. Partial support from KBN 6 P04A 06614 is also acknowledged.

References

1. Kobayashi, M.; Shimizu, S. Nature Biotechnol 1998, 16, 733.
2. Asano, Y.; Tani, Y.; Yamada, H. Agric Biol Chem 1980, 44, 2251.
3. Ashina, Y.; Suto, M. Bioprocess Technol 1993, 16, 91.
4. Kobayashi, M.; Nagasawa, T.; Yamada, H. Trends Biotechnol 1992, 10, 402.
5. Yamada, H.; Kobayashi, M. Biosci Biotechnol Biochem 1996, 60, 1391.
6. Payne, M. S.; Wu, S.; Fallon, R. D.; Tudor, G.; Stieglitz, B.; Turner, I. M. Jr.; Nelson, M. J. Biochemistry 1997, 36, 5447.
7. Hann, E. C.; Eisenberg, A.; Fager, S. K.; Perkins, N. E.;

Gallagher, F. G.; Cooper, S. M.; Gavagan, J. E.; Stieglitz, B.; Hennessey, S. M.; DiCosimo, R. Bioorg Med Chem 1999, 7, 2239.

8. Watt, J. M.; Knowles, C. J. Int Biodeterioration Biodegradation 1995, 227.
9. Tauber, M. M.; Cavaco-Paulo, A.; Robra, K.; Gubitz, G. M. Appl Environ Microbiol 2000, 66, 1634.
10. Nagamune, T.; Kurata, H.; Hirata, M.; Honda, J.; Hirata, A.; Endo, I. Photochem Photobiol 1990, 51, 87.
11. Bonnet, D.; Artaud, I.; Maoli, C.; Petre, D.; Mansuy, D. FEBS Lett 1997, 409, 216.
12. Noguchi, T.; Honda, J.; Nagamune, T.; Sasabe, H.; Inoue, Y.; Endo, I. FEBS Lett 1995, 358, 9.
13. Noguchi, T.; Hoshino, M.; Tsujimura, M.; Odaka, M.; Inoue, Y.; Endo, I. Biochemistry 1996, 35, 16777.
14. Endo, I.; Odaka, M.; Yohda, M. Trends Biotechnol 1999, 17, 244.
15. Huang, W. et al., Structure 1997, 5, 691.
16. Nagashima, S.; Nakasako, M.; Dohmae, N.; Tsujimura, M.; Takio, K.; Odaka, M.; Yohda, M.; Kamiya, N.; Endo, I. Nature Struct Biol 1998, 5, 347.
17. Murakami, T.; Nojiri, M.; Nakayama, H.; Odaka, M.; Yohda, M.; Dohmae, N.; Takio, K.; Nagamune, T.; Endo, I. Protein Sci 2000, 9, 1024.
18. Odaka, M.; Fujii, K.; Hoshino, M.; Noguchi, T.; Tsujimura, M.; Nagashima, S.; Yohda, M.; Nagamune, T.; Inoue, Y.; Endo, I. J Am Chem Soc 1997, 119, 3785.
19. Scarrow, R. C.; Strickler, B. S.; Ellison, J. J.; Shoner, S. C.; Kovacs, J. A.; Cummings, J. G.; Nelson, M. J. J Am Chem Soc 1998, 120, 9237.
20. Hoshino, M.; Laverman, L.; Ford, P. C. Coord Chem Rev 1999, 187, 75.
21. Cerius^{2TM}, BIOSYM/Molecular Simulations, Release 2.0, 1995.
22. Nakasako, M.; Odaka, M.; Yohda, M.; Dohmae, N.; Takio, K.; Kamiya, N.; Endo, I. Biochemistry 1999, 38, 9887.
23. Sugiura, Y.; Kuwahara, J.; Nagasawa, T.; Yamada, H. J Am Chem Soc 1987, 109, 5848.
24. Frisch, M. J.; Trucks, G. W.; Schlegel, H. B.; Scuseria, G. E.; Robb, M. A.; Cheeseman, J. R.; Zakrzewski, V. G.; Montgomery, J. A.; Stratmann, R. E.; Burant, J. C.; Dapprich, S.; Millam, J. M.; Daniels, A. D.; Kudin, K. N.; Strain, M. C.; Farkas, O.; Tomasi, J.; Barone, V.; Cossi, M.; Cammi, R.; Mennucci, B.; Pomelli, C.; Adamo, C.; Clifford, C.; Ochterski, J.; Petersson, G. A.; Ayala, P. Y.; Cui, Q.; Morokuma, K.; Malick, D. K.; Rabuck, A. D.; Raghavachari, K.; Foresman, J. B.; Cioslowski, J.; Ortiz, J. V.; Stefanov, B. B.; Liu, G.; Liashenko, A.; Piskorz, P.; Komaromi, I.; Gomperts, R.; Martin, R. L.; Fox, D. J.; Keith, T.; Al-Laham, M. A.; Peng, C. Y.; Nanayakkara, A.; Gonzalez, C.; Challacombe, M.; Gill, P. M. W.; Johnson, B. G.; Chen, W.; Wong, M. W.; Andres, J. L.; Head-Gordon, M.; Replogle, E. S.; Pople, J. A. Gaussian 98; Gaussian: Pittsburgh, 1998.
25. Becke, A. D. J Chem Phys 1993, 98, 5648.
26. Stevens, P. J.; Devlin, F. J.; Chablowski, C. F.; Frish, M. J. J Phys Chem 1994, 98, 11623.
27. Becke, A. D. Phys Rev A 1988, 38, 3098.
28. Lee, C.; Yang, W.; Parr, R. G. Phys Rev B 1988, 37, 785.
29. Vosko, S. H.; Wilk, L.; Nusair, M. Can J Chem 1980, 58, 1200.
30. Siegbahn, P. E. M.; Blomberg, M. R. A. Annu Rev Phys Chem 1999, 50, 221.
31. Huzinaga, S.; Andzelm, J.; Klobukowski, M.; Radzio-Andzelm, E.; Sakai, E.; Takewaki, H. *Gaussian Basis Sets for Molecular Calculations;* Elsevier: New York, 1984.
32. Hay, P. J. J Chem Phys 1977, 66, 4377.
33. Pou-Amerigo, R.; Merchan, M.; Nebot-Gil, I.; Widmark, P. O.; Roos, B. Theor Chim Acta 1995, 92, 149.
34. Dunning, T. H.; Hay, P. J. *Gaussian Basis Sets for Molecular Calculations.* In Schaefer, H. F., III (Ed.), *Methods of Electronic Structure Theory.* Plenum: New York and London, 1977. p. 1.
35. Noveron, J. C.; Olmstead, M. M.; Mascharak, P. K. Inorg Chem 1998, 37, 1138.
36. Silver, J.; Marsh, P. J.; Symons, M. C. R.; Svistunenko, D. A.; Frampton, C. S.; Fern, G. R. Inorg Chem 2000, 39, 2874.
37. Methods of Enzymology, Vol. 143 (1987) p. 271.
38. Tyler, L. A.; Noveron, J. C.; Olmstead, M. M.; Mascharak, P. K. Inorg Chem 1999, 38, 616.
39. Kozlowski, P. M.; Spiro, T. G.; Berces, A.; Zgierski, M. Z. J Phys Chem B 1998, 102, 2601.
40. Schaftenaar, G.; Noordik, J. H. J Comput-Aided Mol Design 2000, 14, 123.
41. Artaud, I.; Chatel, S.; Chauvin, A. S.; Bonnet, D.; Kopf, M. A.; Leduc, P. Coord Chem Rev 1999, 192, 577.
42. Endo, I.; Nojiri, M.; Tsujimura, M.; Nakasako, M.; Nagashima, S.; Yohda, M.; Odaka, M. J Inorgan Biochem 2001, 83, 247.
43. Piersma, S. R.; Nojiri, M.; Tsujimura, M.; Noguchi, T.; Odaka, M.; Yohda, M.; Inoue, Y.; Endo, I. J Inorg Biochem 2000, 80, 283.